Experimental and computational insights into the aminopropylphosphonic acid modification of mesoporous TiO_2 powder : the role of the amine functionality on the surface interaction and coordination

Experimental and Computational Insights Into the Aminopropylphosphonic Acid Modification of Mesoporous TiO_2 Powder: The Role of the Amine Functionality on the Surface Interaction and Coordination

Nick Gys[a,b], Laurens Siemons[c], Bram Pawlak[d], Kenny Wyns[a], Kitty Baert[e], Tom Hauffman[e], Peter Adriaensens[d], Frank Blockhuys[c], Bart Michielsen[a], Steven Mullens[a], Vera Meynen[a,b]

[a]Sustainable Materials Management, Flemish Institute for Technological Research (VITO NV), Boeretang 200, 2400 Mol, Belgium.
[b]Laboratory of Adsorption and Catalysis (LADCA), Department of Chemistry, University of Antwerp, Universiteitsplein 1, 2610 Wilrijk, Belgium.
[c]Structural Chemistry Group, Department of Chemistry, University of Antwerp, Groenenborgerlaan 171, 2020 Antwerpen, Belgium.
[d]Analytical and Circular Chemistry (ACC), Institute for Materials Research (IMO), University of Hasselt, Agoralaan 1, 3590 Diepenbeek, Belgium.
[e]Research Group Electrochemical and Surface Engineering (SURF), Department Materials and Chemistry, Vrije Universiteit Brussel, Pleinlaan 2, 1050 Brussels, Belgium.

Abstract

Recently, interest has been directed towards the grafting of metal oxides with organophosphonic acids bearing terminal amine groups to extend the functionality and applicability of these materials. Previous reports mainly focus on the application perspective, while a detailed characterization of the surface properties at the molecular level and the correlation with the synthesis conditions are missing. In this work, mesoporous TiO_2 powder is grafted with 3-aminopropylphosphonic acid (3APPA) under different concentrations (20, 75, 150 mM) and temperatures (50, 90 °C) and compared with propylphosphonic acid (3PPA) grafting to unambiguously reveal the impact of the amine group on the surface properties. A combination of complementary spectroscopic techniques and Density Functional Theory - Periodic Boundary Conditions (DFT/PBC) calculations are used. At 90 °C and high concentrations, lower modification degrees are obtained for 3APPA compared to

3PPA, due to amine-induced surface interactions. Both X-ray Photoelectron Spectroscopy (XPS) and Diffuse Reflectance Infrared Fourier Transform (DRIFT) spectroscopy reveal that both NH_2 and NH_3^+ groups are present, with also contributions of NH_2 groups involved in hydrogen bonding interactions. A similar ratio of NH_2/NH_3^+ (65:35) is obtained irrespective of the modification conditions, suggesting similar relative contributions of different surface conformations. Calculated adsorption energies from DFT calculations on 3APPA adsorption on anatase (101) in relation to the water coverage reveals a coexistence of various structures with the amine group involved in intra-adsorbate, inter-adsorbate and adsorbate-surface interactions. Further validation is obtained from the strong overlap of different ^{31}P environments represented by the broad band (35-12 ppm) in experimental ^{31}P Nuclear Magnetic Resonance (NMR) spectra and calculated ^{31}P chemical shifts of all modelled monodentate and bidentate structures. Structures related to the tridentate binding mode are not formed due to geometric restrictions of the anatase (101) facet applied as model support in the calculations. Nevertheless, they could be present in the experimental samples as they are composed of anatase (representing multiple crystal facets) and an amorphous titania fraction.

Keywords: titanium dioxide, 3-aminopropylphosphonic acid, surface modification, synthesis-properties correlation

1. Introduction

Tailoring and altering the surface properties of metal oxides is relevant to a large variety of research domains such as heterogenous catalysis[1,2], selective metal sorption[3–5], separation processes[6,7], cancer therapy[8,9,10] and controlled drug delivery.[11,12,13] The surface of metal oxides mainly consists of M–O–M (in which M is a metal) bonds and surface M–OH groups of different bond strengths and configurations that highly depend on the material

composition, synthesis and post-treatments. Although the surface M–OH chemistry (number, distribution, coordination) can be varied to some extent during (post-)synthesis, the diversity of possible and specific interactions with the environment is limited. Therefore, organic molecules are introduced onto the surface of metal oxides through grafting, to combine the large versatility of functional properties of organic molecules with the structural and chemical properties and mechanical stability of metal oxides. Such hybrid organic-inorganic materials provide the ability to specifically tune the surface properties for an increased control and selectivity of interactions relevant to a particular application.

Although the synthesis and grafting of mesostructured SiO_2 materials is by far the best documented in literature[14,15], non-siliceous mesoporous transition metal oxides (e.g. TiO_2, ZrO_2, Al_2O_3, ZnO, ITO) are gaining interest as well as their use in a wide variety of solvents and pH ranges.[16,17,18] Especially TiO_2 is extensively studied due to the possibilities it offers for the synthesis of a large variety of nano-morphologies and its applications in a wide range of fields.[19–22] Different precursors can be used for grafting transition metal oxides such as organosilanes, organophosphonic acids, carboxylic acids, alcohols and Grignard reagents.[23,24,25,26] Whereas organosilanes are the most applied precursors for surface grafting, in particular for SiO_2, they are less applicable to TiO_2 and ZrO_2, as the poor hydrolytic stability of Ti-O-Si and Zr-O-Si bonds results in a rapid leaching of the organic layer.[27] Grafting long, hydrophobic functional groups and ensuring full surface coverage increases the stability, but reduces to some extent the tailoring of the surface properties relative to other grafting methodologies and limits the applicability of such materials.

Organophosphonic acids (PAs) are a promising alternative for the grafting of metal oxide surfaces, as discussed in various reviews[28–30] and by the study of PA-modified materials in a

variety of technological domains such as membrane separation[6,7,31], supported metal catalysis[32–34,35], hybrid (photo)electric devices[36], implant materials[10,13] and chromatography.[37–40] In contrast to organosilanes, PAs are much less susceptible towards self-condensation (i.e. P–O–P formation) making grafting in water possible, enabling sub-monolayer surface coverage and avoiding the formation of disordered multilayers.[41,42] Grafting of PAs to the surface involves the formation of M–O–P bonds via condensation between P–OH groups and surface M–OH groups, while the phosphoryl oxygen (P=O) can coordinate to Lewis acidic sites. Different bonding types can be envisaged, being mono- , bi- and tridentate. In practice, however, many bonding variants can coexist depending on which and how many reactive groups (P–OH or P=O) bind to the surface and whether the binding is bridging or chelating.[23] Furthermore, unbound P–OH or P=O groups can be involved in hydrogen bonding with adjacent PA groups or with surface hydroxyl groups.

Infrared spectroscopy and ^{31}P solid state NMR are powerful experimental techniques to characterize the grafting of PAs on TiO_2. However, to elucidate the precise binding modes at the surface remains difficult. This is due to the absence of a proper reference set for the vibrational frequencies associated with the Ti–O–P bonds and the strong overlapping absorption band of TiO_2. In a number of occasions this has led to questionable assignments of bands associated with particular binding modes. Moreover, the presence of a broad asymmetric resonance signal in ^{31}P Cross Polarization Magic Angle Spinning (CP/MAS) NMR upon grafting of alkyl PAs suggests that multiple binding modes can coexist with minor differences in P environment. Here, the ^{31}P resonance is also affected by variations in O–P–O bond angles or hydrogen bonding and other non-covalent interactions.[43] Therefore, without reference data, such as those obtained from computations, the identification of the most stable binding modes and structures at the surface and the associated peak assignments

in both ^{31}P NMR and IR is challenging. The strength of computational approaches to support experimental observations has been illustrated by the work of Geldof et al.[44] on the grafting of alkyl PAs on pristine anatase (101) and (001). Irrespective of the alkyl chain length, only a small difference in adsorption energy between mono- and bidentate (i.e. the most stable binding modes) was found, suggesting that both binding modes coexist on the surface. Although their model was limited to pristine ideal surfaces, the results were in good agreement with the broad peaks observed in experimental ^{31}P CP/MAS NMR spectra of alkylphosphonic acid grafted titania. Furthermore, the calculated ^{31}P chemical shifts were in line with the experimental values. A similar study was also reported for the adsorption of phosphate species on anatase.[45]

Previous experimental[43,46–54] and computational[55–58] studies of the PA grafting on TiO_2 have been largely devoted to aliphatic and aromatic PAs. It is known that the modification conditions (temperature, concentration, solvent), type of PA and support properties (crystal phases and facets) strongly affect the properties of the modified surface.[59,60] Guerrero et al.[61] modified P25 with an aqueous solution of phenylphosphonic acid (PhPA) and observed an increase in phosphorus content with increasing temperature. They also described a dissolution-precipitation reaction at the surface (i.e. titanium phenylphosphonate formation) above 100 °C. Following Kickelbick et al.[62], a higher grafting density and alkyl-chain ordering was found for the grafting of ZrO_2 with increasing concentration of dodecylphosphonic acid (DDPA). In a more elaborate study on Al_2O_3[49], an increasing broadening of the ^{31}P NMR resonance signals was observed upon higher octylphosphonic acid loading, indicating relative changes in the binding modes. More recently, the work of Roevens et al.[59,60] provided systematic insight into the role of the modification conditions on the grafting of TiO_2 (P25) with propyl- and phenylphosphonic acid in water and toluene.

They concluded that the synthesis conditions allow the control of the number and distribution of grafted organic groups and possibly the formation of titanium phosphonate.

To extend the functionality and applicability of phosphonic acids, interest has been directed towards the grafting of PAs bearing terminal NH_2 groups on various metal oxides: Fe_3O_4[63–65], TiO_2[66–69], Al_2O_3[70,71], $BaTiO_3$[72] and ZnO.[73] Caruso et al.[66] studied the CO_2 adsorption performance of amine-modified mesoporous TiO_2 beads, using aminomethylphosphonic acid (AMPA), 2-aminoethylphosphonic acid (2AEPA) and 3-aminopropylphosphonic acid (3APPA). Successful grafting was confirmed by an analysis of the P–O region of the vibrational spectra (1300-900 cm^{-1}), but modification degrees were below the detection limit of elemental analysis. In the field of drug delivery and multimodal theranostic applications, Tudisco et al.[64,65] modified magnetic Fe_3O_4 nanoparticles with 3APPA. Based on XPS N1s spectra, NH_2 groups were found in at least two different chemical environments suggesting the presence of different conformations at the surface. The group of Kessler et al.[67], on the other hand, performed a more detailed analysis to determine the presence of grafted groups and the binding mode of 2AEPA on modified titania nanofibers using ^{31}P NMR spectra, in which they identified a broad band at around 20 ppm. However, all the aforementioned studies tend to focus primarily on the application perspective while a detailed and systematic characterization of the modified surface and its correlation to the synthesis conditions is missing. Moreover, further insights and evidence of specific conformations of the grafted amine-bearing groups at the molecular level is lacking in literature.

This article aims to elucidate the impact of the amine group on the grafting of 3APPA on mesoporous TiO_2 (Hombikat M311) and the obtained surface properties. Using propylphosphonic acid (3PPA) as amine-free analogue and, through grafting at different concentrations (20, 75, 150 mM) and temperatures (50, 90 °C) in combination with

characterization and computation, insights are provided on the impact of the amine group on the modification degree, chemical state(s) of NH_2, the aminopropyl conformations and the presence of grafting vs. phosphonate formation. The surface properties of the grafted samples are characterized via a combination of complementary analysis techniques, including DRIFT, XPS and ^{31}P-CP/MAS NMR. This is supported by DFT/PBC calculations to gain insights into the different surface conformations, based on calculated adsorption energies and a structural analysis, and calculated ^{31}P chemical shifts that are correlated to the experimental findings. This work contributes to a better understanding of amine-containing organophosphonic acid modified TiO_2 materials. Since material synthesis and application are highly correlated, insights into surface properties and their correlation to synthesis conditions, provide important know-how towards their use and performance in applications.

2. Experimental Section

2.1 Materials

3-Aminopropylphosphonic acid hydrochloride salt (3APPA) and propylphosphonic acid (3PPA) were purchased from Sikémia. Mesoporous TiO_2 Hombikat M311 (crystal phase:100% anatase, BET surface of 300-350m²/g) was supplied by Sachtleben Chemie GmbH (now VENATOR) and used without pre-treatment.

2.2 Surface modification

2.0 g of Hombikat M311 was stirred under reflux for 4 hours in a heated aqueous solution of 50 ml 3APPA or 3PPA. Both the concentration (20, 75 and 150 mM) and temperature (50 and 90 °C) were varied. After modification, the samples were washed by pressure filtration to remove unreacted and physisorbed PA. During this process, the reactant solution was removed, followed by batch pressure filtration with 400 mL H_2O for each washing step. After five consecutive washing steps (i.e. total volume of 2 L), the samples were dried overnight in

an oven at 60 °C. The nitrogen and phosphorus concentration in the collected washing eluates were analyzed to evaluate the extent of washing (Figure S1). All samples received structural names indicating the modification conditions, e.g. 3APPA20mM50 representing a sample modified with 20 mM of 3APPA at 50 °C; 3PPA150mM90 represents a sample modified with 150mM of 3PPA at 90 °C.

2.3 Instrumentation

DRIFT measurements were performed on a Nicolet 6700 Fourier Transform IR spectrometer, equipped with an electromagnetic source in the mid-IR region (4000-400 cm^{-1}) and liquid N_2 cooled MCT-B detector. A resolution of 4 cm^{-1} was used and for each spectrum 200 scans were accumulated. Measurements were performed at room temperature under vacuum (30 mbar) after 30 minutes of stabilization time. The sample holder contained a 2 wt% diluted sample in KBr.

Inductively Coupled Plasma Atomic Emission Spectroscopy (ICP-AES, Agilent Technologies 5100 ICP-OES) was performed to determine the P content of the 3APPA and PPA modified samples. Samples were digested in a solution of 1.5 ml HNO_3 (67-69 %), 1.5 ml HF (48 %) and 3 ml H_2SO_4 (96 %) for 24 hours at 250 °C. After digestion, 16 ml H_3BO_3 (4%) was added to neutralize the HF. The modification degree in number of grafted groups per nm² (#groups/nm²) is calculated from the weight percentage of P using the following formula:

$$mod.degr.\left(\frac{\#}{nm^2}\right) = \frac{wt\ \%(P) \times N_A}{MM(P) \times S_{BET}}$$

in which wt%(P) is the weight percentage of P, MM (P) is the molar mass of P, S_{BET} is the surface area of the unmodified TiO_2 powder and N_A is Avogadro's constant. The

experimental error is estimated to be 0.1 groups/nm² based on four repeated modifications at fixed synthesis conditions.

N_2 sorption measurements were performed at -196 °C using a Quantachrome Quadrasorb SI automated gas adsorption system. Prior to the measurements, the samples were degassed for 16 hours under high vacuum at 200 °C. The specific surface area was calculated by the BET (Brunauer-Emmett-Teller) method. The measured apparent BET surface area is 300 m²/g (± 30 m²/g) based upon three measurements. For the sorption isotherm and pore size distribution, the reader is referred to the supplementary information (Figure S2).

XPS spectra were collected using a VersaProbe II photoelectron spectroscope (Physical Electronics) with an Al Kα monochromatic X-ray source (1486.71 eV of photons). The vacuum in the analysis chamber was approximately 5×10^{-7} Pa during measurements. High-resolution scans of the Ti2p, O1s, C1s, P2p and N1s photoelectron peaks were recorded from a spot diameter of 100 µm using a pass energy of 23.4 eV and a step size of 0.1 eV. Measurements were performed with a takeoff angle of 45° with respect to the sample surface. The powders were applied on indium foil. Data was analyzed with PHI Multipak software. Prior to curve fitting, the energy scale of the XPS spectra was calibrated relative to the binding energy of Ti $2p_{3/2}$ (458.5 eV) for 3APPA and 3PPA grafted samples, and to advantageous hydrocarbons (C-C/C-H) in the C1s peak at 284.7 eV for the 3APPA and 3PPA precursors. Curve fitting was done after a Shirley type background removal, using mixed Gaussian (80–100%) – Lorentzian shapes. For relative quantification of the different components in the N1s spectra, the area of the fitted peaks was used.

Phosphorus-31 solid-state CP/MAS NMR spectra were acquired at ambient temperature on an Agilent VNMRS DirectDrive 400 MHz spectrometer (9.4 T wide bore magnet) equipped

with a T3HX 3.2 mm VT probe dedicated for small sample volumes and high decoupling powers. Magic angle spinning (MAS) was performed at 15 kHz using ceramic zirconia rotors of 3.2 mm in diameter (22 μL rotors). The phosphorus chemical shift scale was calibrated to orthophosphoric acid (H_3PO_4) at 0 ppm. Other acquisition parameters used were: a spectral width of 60 kHz, a 90° pulse length of 3.2 μs, a spin-lock field for CP of 80 kHz, a contact time for CP of 0.9 ms, an acquisition time of 15 ms, a recycle delay time of 4 s and 512 accumulations. High power proton dipolar decoupling during the acquisition time was set at 80 kHz. The Hartmann-Hahn condition for CP was calibrated accurately on the samples themselves.

2.4 Quantum chemical calculations

All calculations were performed under Periodic Boundary Conditions (PBC) with the Quantum Espresso (QE) software package[74] using plane waves as basis sets. The Wu & Cohen (WC) modification of the PBE functional[75] was used since it allows for a high-quality description of solid-state materials.[76] Treatment of the core electrons is based on the Projector Augmented Wave (PAW) method.[77] The $1s^2$ electrons are treated as core electrons for C, O and N, whereas the $1s^22s^22p^6$ electrons are treated as core electrons for Ti and P. An energy cutoff of 60 Ry and a k-point grid of $2 \times 2 \times 1$ were used. Dispersion interactions were taken into account by adding an additional term to the DFT total energy based on the DFT-D2 method by Grimme.[78,79] The anatase (101) facet was selected in the model since this is the most exposed facet in the anatase crystal phase of Hombikat M311 titania powder (Figure S3, Table S1). A 3-layer slab with a 20 Å vacuum width was constructed using the cif2cell software package[80] and functionalized with 3-aminopropyl phosphonic acid. Taken into account the dimensions of the slab, the presence of one 3APPA molecule corresponds to a surface coverage of about 0.9 groups/nm^2. The atoms in the lowest layer of the slab were constrained to their initial bulk positions, while all other atoms were allowed to relax.

Calculations of the ^{31}P chemical shifts were performed using the Gauge-Including Projector Augmented Wave (GIPAW) method[81], as implemented in the QE software package. The isotropic chemical shift δ_{iso} is defined as $\delta_{iso} = -(\sigma - \sigma_{ref})$, but in order to compare experimental and calculated chemical shifts, the isotropic shielding of the reference needs to be carefully selected. Berlinite ($AlPO_4$) with $\delta_{iso}(^{31}P) = -25.6$ ppm[82] referenced to H_3PO_4 was chosen to define $\sigma_{ref,calc}(^{31}P)$.

3. Results and discussion

3.1 Evidence of the impact of the amine group on the modification degree and surface bonding

Comparing the modification degree of 3APPA and 3PPA under the studied grafting conditions leads to the first insights into the impact of the NH_2 group on the modification (Table 1). For 3PPA, modification degrees between 0.6 and 1.4 #/nm² are obtained. At both modification temperatures (50 and 90 °C), the modification degree increases with increasing 3PPA concentration. This increase is more pronounced at 90 °C, evidenced by the two-fold increase in modification degree from 3PPA20mM90 (0.7 #/nm²) to 3PPA150mM90 (1.4 #/nm²). In addition, for similar concentrations, modification at 90 °C results in a higher modification degree.

For 3APPA, modification degrees between 0.6 and 1.1 #/nm² are obtained. Similarly to 3PPA, the modification degree increases with increasing concentration and temperature. At 50 °C, similar values of the increase in modification degree are observed as for 3PPA, i.e. ranging from 0.6 to 0.9 #/nm². At 90 °C, however, a first difference with 3PPA is observed. Indeed, a smaller increase in modification degree is observed with increasing concentration from 3APPA20mM90 (0.8 #/nm²) to 3APPA150mM90 (1.1 #/nm²).

Based on these findings, it can be concluded that elevating the concentration of 3APPA or 3PPA and the temperature results in an increased modification degree. For 3PPA, the concomitant effect of a high temperature (90 °C) and a high concentration (75 and 150 mM) strongly promotes achieving higher modification degrees compared to the modifications at 50 °C, where the concentration has less impact on increasing the modification degree. This is in accordance with the work of Roevens et al..[59] Since water is used as solvent, having a high dielectric constant and strong polar interaction with the TiO_2 surface, a competition for adsorption at the surface between the organophosphonic acid and water molecules occurs. Before surface bonding can occur, an organophosphonic acid has to displace water molecules from the surface. At 50 °C, this competition is stronger and thus makes it difficult to achieve high modification degrees, even if high concentrations are used. The effect of the temperature on the modification degree for 3APPA is, however, less pronounced which indicates that also other effects/mechanisms seem to occur next to the above mentioned competition with water.

Table 1: Calculated modification degree from ICP-AES analysis for Hombikat M311 modified with different concentrations of 3APPA and PPA in water at 50 °C and 90 °C, expressed as number of grafted groups per nm² (#/nm²).

T (°C)	C (mM)	3APPA (#/nm²)	3PPA (#/nm²)
50	20	0.6	0.6
	75	0.7	0.8
	150	0.9	0.9
90	20	0.8	0.7
	75	0.9	1.1
	150	1.1	1.4

DRIFT analysis confirms the successful bonding and presence of 3APPA groups on the TiO_2 surface, as shown in Figure 1. Large similarities in the P–O regions (1300-900 cm^{-1}) of 3APPA20mM50 and 3APPA150mM50 are found, characterized by a superposition of at least three broad absorption bands at 1122, 1042 and 990 cm^{-1}, although slight differences in the broadness/sharpness of the bands at 1122 and 990 cm^{-1} relative to the other signals can be observed. For 150 mM, these peaks seem broadened and less pronounced than for 20 mM. No visible impact of the temperature is observed, since a similar broadening is present at 90 °C (Figure 2). Secondly, the comparison between the 3APPA and 3PPA modifications at 20 and 150 mM reveals clear differences in surface bonding (Figure 1). For the sake of simplicity and without affecting the main conclusions, only the modifications at 50 °C are shown and discussed. Considering the P–O region of 3PPA20mM50 and 3PPA150mM50, not only the positions of the absorption bands are shifted compared to 3APPA, also the relative intensities and broadness of the bands are different. In the region of the band of 3APPA centered at 990 cm^{-1}, two (partly) overlapping absorption bands at around 1000 cm^{-1} and 970 cm^{-1} are visible for 3PPA, while the relative intensity at 990 cm^{-1} seems to decrease. In addition, the band at 1122 cm^{-1} of 3APPA is shifted to a lower wavenumber for 3PPA and the broad undefined band at 1042 cm^{-1} becomes more pronounced and resolved for 3PPA.

At higher wavenumbers, in the region between 1250 and 1200 cm^{-1}, a clear peak is visible at 1242 cm^{-1} with a similar intensity and broadness for both 3PPA20mM50 and 3PPA150mM50. For the corresponding 3APPA samples, this signal is almost not visible. The assignment of this peak and the interpretation of its absence in terms of the binding modes of this peak, has been the subject of controversy in literature. In numerous studies, the tridentate binding mode is proposed as the predominant binding mode in the absence of this P=O absorption band.[42,61,83–86] However, quantum chemical calculations point to the fact that

mono- and bidentate binding modes involve the coordination of the doubly-bound phosphoryl oxygen atom towards a surface Ti atom.[44,55–57] This results in an increase in the P–O bond length which is reflected in a considerable shift of the P=O stretch to a lower wavenumber. Consequently, the assignment of the presence or absence of the signal at 1242 cm^{-1} remains uncertain. Despite this, the aforementioned differences in the P–O region between 3PPA and 3APPA strongly suggest differences in interface chemistry for both type of modifications. This can be explained due to the fact that P–O peak positions are strongly affected by the degree of metal bonding and other non-covalent interactions such as hydrogen bonding.

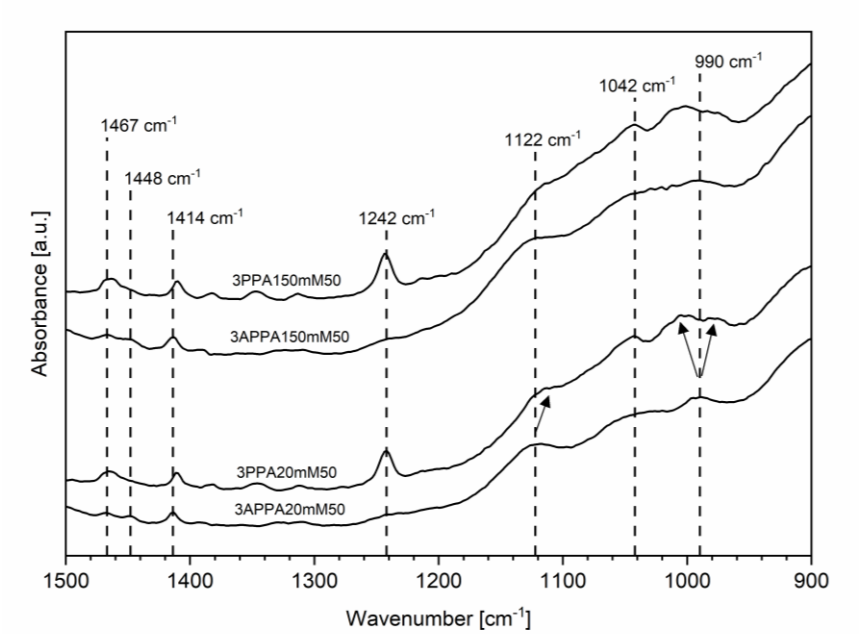

Figure 1: DRIFT spectra (1500-900 cm^{-1}) of 3APPA and 3PPA grafted samples modified at 20 and 150 mM at 50 °C. Offset has been used to visualize the spectra more clearly.

In the alkyl deformation region (1500-1400 cm^{-1}) of 3APPA20mM50 and 3APPA150mM50 (Figure 1), three signals at 1467, 1448 and 1414 cm^{-1} are visible since each methylene group in the aminopropyl chain is in a different chemical environment. The two signals at 1467 and 1448 cm^{-1} are commonly assigned to the methylene groups closest to the of NH_2 moiety. [87,88] The signal at 1414 cm^{-1} can then be assigned to the deformation vibration of the CH_2– bound to P. [88]A small shift of this signal to a lower wavenumber (1410 cm^{-1}) is observed for

3PPA20mM50 and 3PPA150mM50. Since the positions of methylene deformation vibrations are susceptible to the conformational mobility within and/or between the organic chains, this possibly also highlights differences in this aspect between 3APPA and 3PPA.

3.2 Chemical state(s) of the amine group

To gain insight into the presence of the different possible chemical state(s) of the NH_2 group, and the different surface conformations of 3APPA associated with those states, complementary information has been obtained via DRIFT and XPS. The 3APPA samples modified at the lowest (20 mM) and highest concentrations (150 mM) at both temperatures (50 and 90 °C) have been analyzed. Figure 2 shows the corresponding DRIFT spectra between 1800 and 900 cm^{-1}, including the native support. The bending vibration of NH_2 (1582 cm^{-1}) is only visible as a shoulder on the deformation mode of molecular adsorbed water[89,90] at 1622 cm^{-1}. In addition, a broad band between 1540 and 1490 cm^{-1}, which is centered around 1525 cm^{-1}, can be assigned to the asymmetric deformation vibration of NH_3^+ groups.[91–94] The position of the NH_2 band is shifted to lower wavenumbers compared to those typical for these vibrations for aqueous solutions of primary amines (around 1600 cm^{-1}).[95] This shift can be attributed to hydrogen bonding interactions of the NH_2 group in which the nitrogen atom is involved as hydrogen acceptor. [91] Indeed, similar shifts (from 1600 to about 1575 cm^{-1}) have been typically reported for aminopropylsiloxane polymers and 3-aminopropyltriethyoxysilane (APTES) grafted silica.[95–98] This is a result of interactions between amine and silanol groups resulting in a variety of hydrogen-bonded surface conformations such as an intramolecular 6-membered ring structure.

In this work, the presence of unbound P–OH groups in addition to surface hydroxyl groups (Ti–OH) available for hydrogen bonding and or acid/base interactions further complicates the unraveling of the possible interaction of the amine group on the surface. Clearly, 3APPA

forms a disordered surface chemistry with a variety of conformations upon bonding on Hombikat. Unfortunately, the interference of adsorbed water on the surface hampers the determination of the relative contributions of the amine speciation.

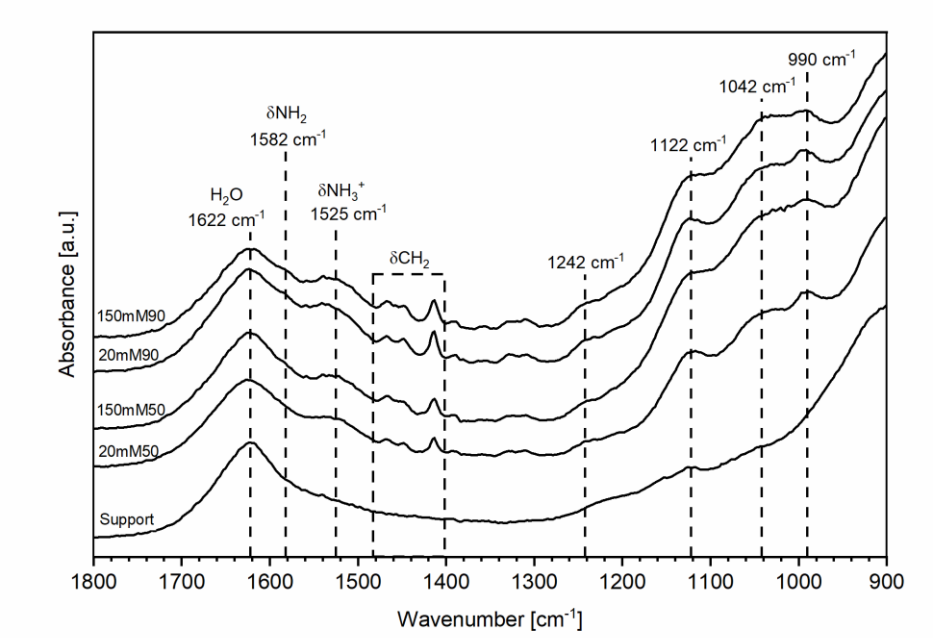

Figure 2: DRIFT spectra (1800-800 cm^{-1}) of the native and 3APPA grafted samples. Offset has been used to visualize the spectra more clearly.

Semi-quantitative information on the amine speciation is obtained from the high resolution N1s XPS spectra of the precursor, the native and 3APPA grafted samples as shown in Figure 3. For the native support (Figure 3B), a peak at 399.8 eV is observed which originates from traces of molecularly adsorbed N_2.[99–101] The N1s spectrum of 3APPA (Figure 3A) consists of a single peak at 401.0 eV. Since 3APPA is a HCl salt, this peak can be attributed to NH_3^+ groups present as $NH_3^+Cl^-$. Upon grafting, the N1s spectra of all the modified samples consist of a broad asymmetric band composed of two contributions at 399.6 (±0.1) and 401.4 (±0.1) eV after peak deconvolution (Figure 3C). The complicating factor in N1s data interpretation is that different types of interactions can have a similar binding energy. [102,103,104] The component at low binding energy (399.6 eV) can be assigned to non-interacting NH_2 groups or to Lewis acid-base interactions, in which there is a donation of the lone-pair electron

density of nitrogen to surface Ti sites.[105] It is a general rule that, the higher the partial charge on nitrogen, the higher the binding energy. Hence, the component at high binding energy (401.4 eV) is commonly assigned to protonated NH_3^+ groups, originating from proton transfer with hydroxyl groups (e.g. P–OH, Ti–OH, adsorbed water). Hydrogen bonded amine groups are experimentally difficult to observed by XPS, and although commonly assigned to similar binding energies as NH_3^+, the precise binding energy and its contribution to the broad asymmetric N1s signal logically depends on its interaction strength.

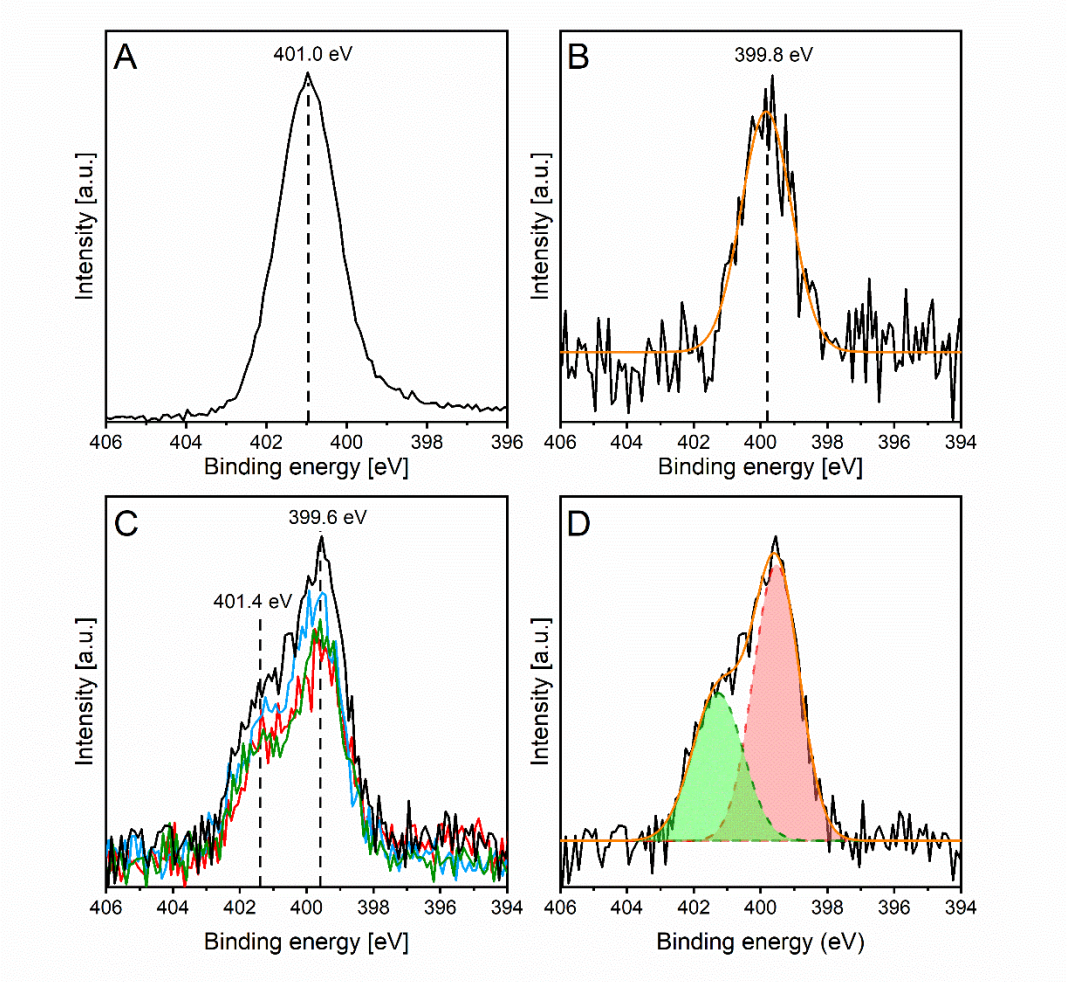

Figure 3: N1s spectra of A) 3APPA precursor, B) Hombikat M311 support, C) grafted 3APPA samples at two concentrations (20 and 150 mM) and two temperatures (50 and 90 °C) and D) peak fitted spectrum of 3APPA150mM90. Red: 3APPA20mM50, blue: 3APPA150mM50, green: 3APPA20mM90 and black: 3APPA150mM90

Peak fitting of the spectra results in a NH_3^+/NH_2 ratio of 35%/65% (±2%) irrespective of the concentration and temperature, and therefore, the peak fitted spectrum of one synthesis condition (i.e. 3APPA150mM90) is shown in Figure 3D. The N1s peak positions are sensitive to changes in surface energy such as changes in neighboring atoms and interaction strengths. Given the similar peak positions and ratio of NH_2 and NH_3^+ for all samples, this suggests that the relative contributions of specific surface arrangements of grafted 3APPA are quite similar for all samples, as far as they have sufficient difference in surface energy since different 3APPA conformations can result in similar N1s peak positions. Based on the above results, many possible surface conformations of 3APPA on Hombikat can be envisaged, including free NH_2 groups accessible for interactions with their surroundings and NH_2 groups involved in intra- and inter-adsorbate interactions and adsorbate-surface interactions, with the adsorbate being the 3APPA.

3.3 Surface interactions and conformations of 3APPA

Despite the experimental evidence that a 3APPA modified TiO_2 surface is composed of different conformations, further details of these conformations at the molecular level are lacking. Therefore, DFT calculations have been performed to investigate the various interaction possibilities of the amine group, the different binding modes (mono-, bi- and tridentate) and the adsorption energy of each conformation. Modelling of 3APPA grafting is performed on the (101) anatase facet which is known to be the thermodynamically most stable and most abundant crystal facet in anatase.[44] In the supplementary information, the peak fitting of the (101) and (004) XRD diffraction peaks of the Hombikat support can be found. The (004) signal is representative for the (001) facet, and resulted in a (101)/(001) ratio of 88/12. This supports the decision to perform the DFT calculations on the anatase (101) facet.

3.3.1 Clean anatase (101)

Initially, DFT calculations were performed on a clean (101) surface, i.e. only the surface and 3APPA are considered and calculated in vacuum. The adsorption energies (E_{ads}) are calculated as $E_{ads} = E_{(adsorbate + surface)} - (E_{adsorbate} + E_{surface})$, where $E_{(adsorbate + surface)}$ is the energy of the adsorption complex, while $E_{adsorbate}$ and $E_{surface}$ are the energies of the isolated 3APPA molecule and the clean surface, respectively. First, the different binding modes of 3APPA with non-interacting NH_2 groups were modelled: a monodentate structure with two hydrogen bonds involving the bridging oxygens of the anatase facet (-228.24 kJ/mol, structure **1** in Figure 4), and a bidentate structure (-235.82 kJ/mol, structure **2** in Figure 4) in which one P–OH group is involved in a hydrogen bond while the other has lost its hydrogen atom to a neighboring bridging oxygen. The energy difference between both binding modes and structures is small (less than 10%) suggesting that both coexist on the surface. It should be noted that the tridentate structure was not considered in the calculations, since the particular geometry of the anatase (101) surface prevents its formation.

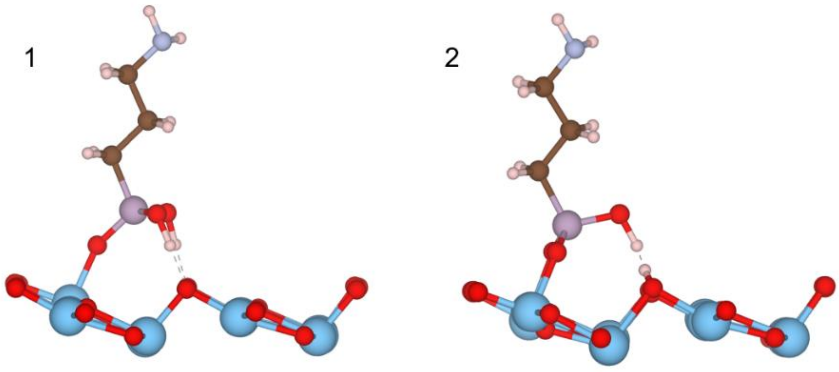

Figure 4: Optimized calculated geometries of the monodentate (**1**) and bidentate structures (**2**) of 3APPA adsorbed on anatase (101) with free, non-interacting NH_2 groups. Red, cyan, pink, brown, white and gray represent oxygen, titanium, phosphorus, carbon, hydrogen and nitrogen atoms, respectively

In comparison, for the amine-free analogue (i.e. 3PPA), adsorption energies of -227.85 kJ/mol and -236.17 kJ/mol are calculated for the monodentate (structure **1-3PPA**) and bidentate (structure **2-3PPA**) binding modes, respectively. The reader is referred to Figure S5 for both structures. Based on the results, a co-existence of both structures on the surface is suggested given the small energy difference, similarly to 3APPA. In addition, for each binding mode (i.e. mono- or bidentate), there is a similar adsorption energy for 3APPA and 3PPA. This suggests a negligible influence of the amine functionality on the adsorption energy, as far as the propyl chains of 3APPA are stretched with the amine group protruding to the environment.

In a next step, the possibility of forming both intra- and inter-adsorbate interactions between the NH_2 and P-OH moieties and inter-adsorbate interactions between two different NH_2 groups was evaluated, starting from monodentate 3APPA. The resulting optimized geometries are shown in Figure 5. Upon formation of an intra-adsorbate N–H…O interaction, the aminopropyl chain is folded towards the surface resulting in a 7-membered ring structure (**3**) in which the amine group acts as hydrogen donor. Alternatively, it can also act as an acceptor in an O–H…N hydrogen bond in **4**. Their energies are -230.32 kJ/mol and -223.55 kJ/mol, respectively. Although there is no proton transfer to form NH_3^+ in either structure, the relatively small H…N distance (1.514 Å) in the latter isomer (**4**) implies the formation of a strong hydrogen bond. Next, when two adsorbates are considered in close proximity, the formation of an N–H…N hydrogen bond between their amine groups with a N–H…N distance of 2.099 Å leads to low-energy conformation **5** (-245.53 kJ/mol). An even more stable situation is found when an inter-adsorbate O–H…N interaction is formed which results in the formation of an NH_3^+ moiety (-271.88 kJ/mol) in **6**. For two adjacent 3PPA adsorbates (structure **5-3PPA**), an adsorption energy of -234.62 kJ/mol is calculated and the structure is

shown in Figure S6. Given the lower adsorption energy of structure **5** of around 11 kJ/mol compared to **5-3PPA**, one can regard this as a measure of the interaction strength between two 3APPA chains.

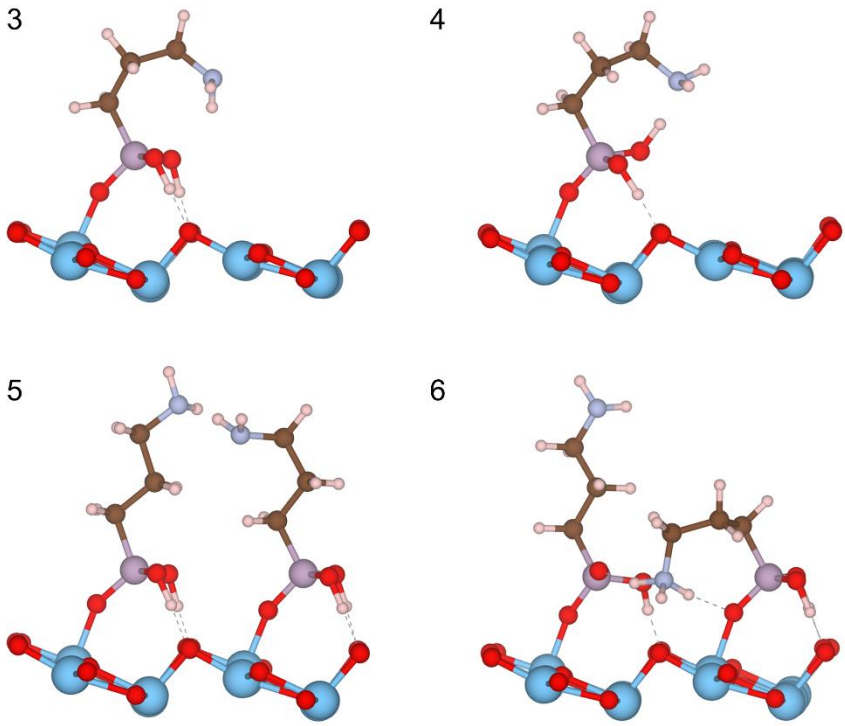

Figure 5: Optimized calculated geometries of 3APPA adsorbed on anatase (101) of the intra-adsorbate N–H…O interaction (**3**), the intra-adsorbate O–H…N interaction (**4**), the inter-adsorbate N–H…N interaction (**5**) and the inter-adsorbate O–H…N interaction (**6**).

3.3.2 Impact of hydrated anatase (101)

In reality, however, the TiO_2 surface can be present in different hydration states depending on the atmospheric and/or measuring conditions. When hydrated, a monolayer of interacting water molecules is presumably always present at the surface. Therefore, the impact of a monolayer of adsorbed water molecules on the adsorption energy of 3APPA and the amine speciation was assessed. The fact that molecular adsorption of H_2O is favored over dissociative adsorption on a defect-free anatase (101) facet has already been described in the literature.[106–109] In a first step, the impact of a single H_2O molecule (i.e. a monohydrated

surface) is evaluated. For all conformations, this results in an overall decrease of up to 20 kJ/mol in adsorption energy and, therefore, stabilization of each calculated geometry. This stabilization is caused by the formation of hydrogen bonds from a neighboring water molecule; the hydrogen atom of a free P–OH group will migrate towards a bridged oxygen, leaving behind an oxygen anion stabilized by a hydrogen bridge with the surrounding water molecule. While no changes in the conformational folding of the aminopropyl chain or in the amine speciation are observed for the conformations already involved in inter- or intra-adsorbate interactions, significant differences are observed for the structures with free, non-interacting NH_2 groups, i.e. those shown in Figure 4.

For the monodentate structure, the presence of a H_2O molecule coordinated to a Ti atom next to grafted 3APPA results in the dissociation of this H_2O molecule in tandem with the formation of a surface hydroxyl group and a NH_3^+ group (structure **7** in Figure 6), via the folding of the aminopropyl chain to the surface. The hydrogen atom of one of the P–OH groups has migrated towards a bridged surface oxygen leaving behind an oxygen anion. This $P–O^-$ anion is stabilized by hydrogen bonding with the resulting surface hydroxyl group which is also taking part in hydrogen bonding with the protonated amine. Although a similar folding occurs for the bidentate structure, an O–H…N hydrogen bond (1.461 Å) is observed between an undissociated H_2O molecule and the amine moiety. The latter is not protonated but engages in an N–H…O hydrogen bond with one of the oxygen atoms of the phosphonic acid group (structure **8** in Figure 6). The adsorption energies of both geometries (-330.77 and -316.61 kJ/mol for **7** and **8**, respectively) are about 35-100 kJ/mol lower than the adsorption energies of the other monohydrated geometries, as shown in Table 2, which gives an overview of the calculated adsorption energies for each geometry in function of water

coverage. This decrease is most likely due to the hydrogen bonding interactions formed which lead to a considerable stabilization of the overall structure.

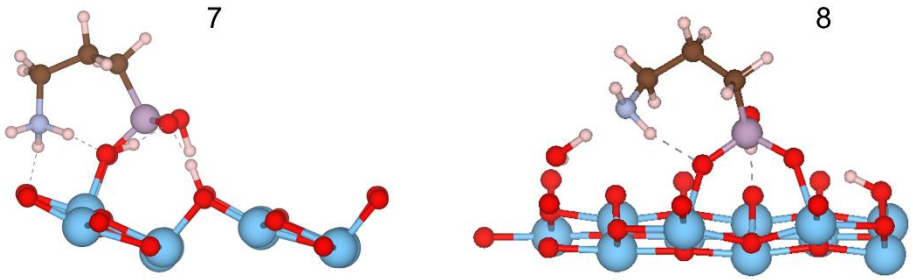

Figure 6: Optimized calculated geometries on monohydrated anatase (101) for the monodentate (**7**) and bidentate (**8**) structures.

In a next step, the number of adsorbed H_2O molecules was increased to full monolayer coverage (i.e., 5 water molecules for monodentate and 4 water molecules for bidentate), which resembles more closely the hydration state under real experimental conditions given the strong absorption band of water as observed in the DRIFT spectra (Figure 2). A further stabilization and consequent decrease in adsorption energy of 10 to 45 kJ/mol was observed for all conformations. For the modeled 3PPA structures without the amine functionality, a similar stabilization is observed, indicating that the presence of water on anatase 101 intrinsically results in a stabilization of the organophosphonic acid adsorption complex, independent on the presence of the amine group. A detailed discussion on the differences in the extent of stabilization goes beyond the objective of this work, and the reader is referred to Figure S7 for a graphical representation on the trends in adsorption energies in function of the hydration degree. Although conformation 7 is slightly favored (-347.73 kJ/mol), a conclusive statement on a preferred conformation is not possible due to minor differences in adsorption energies between the modelled conformations. Both DFT calculations and the experimental results point to the coexistence of multiple conformations at the surface. A decisive

conclusion on the relative contribution of each structure to the surface chemistry of adsorbed 3APPA cannot be drawn.

Table 2: Calculated adsorption energies (kJ/mol) of the different 3APPA and 3PPA surface conformations on a clean, a mono and a fully hydrated anatase (101) facet.

Conformation	Titania-PA interaction	Adsorbate Interaction	E_{ads} clean (kJ/mol)	E_{ads} #1 water (kJ/mol)	E_{ads} #5 water (kJ/mol)
1	Monodentate	none (free NH_2)	-228.24	-248.39	-263.98
2	Bidentate	none (free NH_2)	-235.82	-235.92	-245.46
3	Monodentate	intra N–H…O	-230.32	-251.17	-274.14
4	Monodentate	intra O–H…N	-223.55	-232.62	-277.59
5	Monodentate	inter N–H…N	-245.53	-258.91	-274.71
6	Monodentate	inter O–H…N	-271.88	-281.44	-296.36
7	Monodentate	adsorbate-surface	n.a.	-330.77	-347.73
8	Bidentate	adsorbate-surface	n.a.	-316.61	-314.43
1-3PPA	Monodentate	n.a.	-227.85	n.d.	-263.30
2-3PPA	Bidentate	n.a.	-236.17	n.d.	-248.32
5-3PPA	Monodentate	n.a.	-234.62	n.d.	-264.56

3.4 Binding modes of 3APPA and correlation between experimental and calculated ^{31}P chemical shifts

Based on the calculated adsorption energies, DRIFT and XPS, a large variety of surface conformations can be formed and coexist on the surface depending on the hydration state. Solid-state ^{31}P NMR spectroscopy has been applied and compared with calculated ^{31}P chemical shifts, to gain further experimental insights into the prevalence of these conformations. Figure 7A shows the ^{31}P CP-MAS spectra of 3APPA20mM50 and

3APPA150mM50. Pure 3APPA has a sharp resonance signal at 25.1 ppm, in accordance with previous literature reports.[110,111] Upon binding to the surface, both samples show a broad asymmetric peak between 35 and 12 ppm consisting of at least three overlapping resonances. A main resonance is found at 25.5 ppm with an upfield shoulder around 22 ppm and a less resolved downfield shoulder around 29 ppm. In comparison, the ^{31}P CP-MAS spectra 3PPA20mM50 and 3PPA150mM50 (Figure 7B) also reveal a broad asymmetric peak between 38 and 15 ppm, but with a different shape and pattern than for the 3APPA samples. A main resonance is found at 33 ppm with multiple upfield resonance signals, which become more prominent at 150 mM.

It is clear that this broadening originates from the many small differences between the various electronic environments of the phosphorus atom associated with the many different binding modes and surface conformations present, which is in agreement with the results of the DFT calculations. To be able to correlate the resonance signals with specific 3APPA conformations and/or binding types, the ^{31}P NMR chemical shifts associated with each of the previously optimized structures (clean, mono- and fully hydrated surfaces) were calculated and the results are given in Table 3. In general, increasing the number of adsorbed water molecules from a monohydrated to a fully hydrated surface results in a maximal upfield ^{31}P shift of no more than 4 ppm. Considering the typical broad bands observed in the solid-state NMR spectra, the impact on the P-environment of water as surrounding medium is negligible. Large differences in the calculated ^{31}P shifts between the different 3APPA conformations have been found. A first note should be made concerning the starting conformations of the mono- (**1**) and bidentate (**2**) structures. Although both geometries have a similar adsorption energy, a difference of up to 9 ppm in their ^{31}P chemical shift is found due to the extra bond made with the surface in case of the bidentate structure. The bidentate

structure (31-28 ppm) is shifted downfield with respect to the monodentate structure (24-20 ppm). Compared with 3PPA, similar calculated chemical shifts and trends are found for the bidentate (30-28 ppm) and monodentate structure (23-20 ppm).

Next, the sensitivity of the ^{31}P shift towards subtle changes in the local P-environment can be clearly illustrated via the intra-adsorbate interactions. With respect to structure **1**, the intra-adsorbate N–H…O interaction (**3**) results in a downfield shift of 6 ppm while an upfield shift of 1-5 ppm is observed for **4**. As a result, one can note that intra-adsorbate interactions and the perturbation of one P-OH group towards the NH_2 group has a strong influence on the ^{31}P shift. In order to assess if a similar effect is observed for the bidentate structure (**2**) due to an intra-adsorbate interaction, an additional conformation was modelled (**9**, Figure S8). Peculiarly, a negligible downfield ^{31}P shift of no more than 2 ppm is observed with respect to **2**. Lastly, the interaction between molecularly adsorbed H_2O and NH_2 in **7** induces a 9 ppm upfield ^{31}P shift, most likely due to the multiple hydrogen bonding interactions in the vicinity of the P nucleus. For the inter-adsorbate interactions in structures **5** and **6**, two different ^{31}P chemical shifts are found since the P environment of each 3APPA group is perturbed upon interaction, due to changes in the electron density around the P nucleus (i.e. shielding or deshielding). For example, in structure **6**, the formation of a $P–O^-$ anion upon migration of the hydrogen atom towards the amine group of the adjacent folded 3APPA group, results in shielding of the P atom which is reflected by an upfield shift of 8-14 ppm with respect to isolated monodentate bonded 3APPA (structure **1**).

The calculated ^{31}P NMR chemical shifts of the different structures coincide with the broad band in the experimental spectra, impeding an unambiguous assignment. This is in line with the observations in the calculated adsorption energies and the results obtained in the DRIFT

and XPS spectra. Nevertheless, the broad band is in agreement with the wide range of calculated ^{31}P chemical shifts, indicating that different conformations will co-exist on the surface, all with energies closely related to each other and slightly different P environments.

Table 3: Calculated ^{31}P NMR shifts (ppm) of the different 3APPA and 3PPA surface conformations on a clean, mono- and fully hydrated anatase (101) facet.

Conformation	Titania-PA interaction	Adsorbate Interaction	Clean	#1 H_2O	#5 H_2O
1	Monodentate	none (Free NH_2)	24	22	20
2	Bidentate	none (Free NH_2)	30	31	28
3	Monodentate	intra N–H…O	30	28	26
4	Monodentate	intra O–H…N	19	19	19
5	Monodentate	inter N–H…N	23 and 30	20 and 30	20 and 28
6	Monodentate	inter O–H…N	10 and 24	12 and 23	12 and 21
7	Monodentate	adsorbate-surface	n.a.	19	15
8	Bidentate	adsorbate-surface	n.a.	23	19
9	Bidentate	intra N–H…O	32	n.d.	28
1-3PPA	Monodentate	n.a.	23	n.d.	20
2-3PPA	Bidentate	n.a.	30	n.d.	28
5-3PPA	Monodentate	n.a.	23 and 23	n.d.	21 and 21

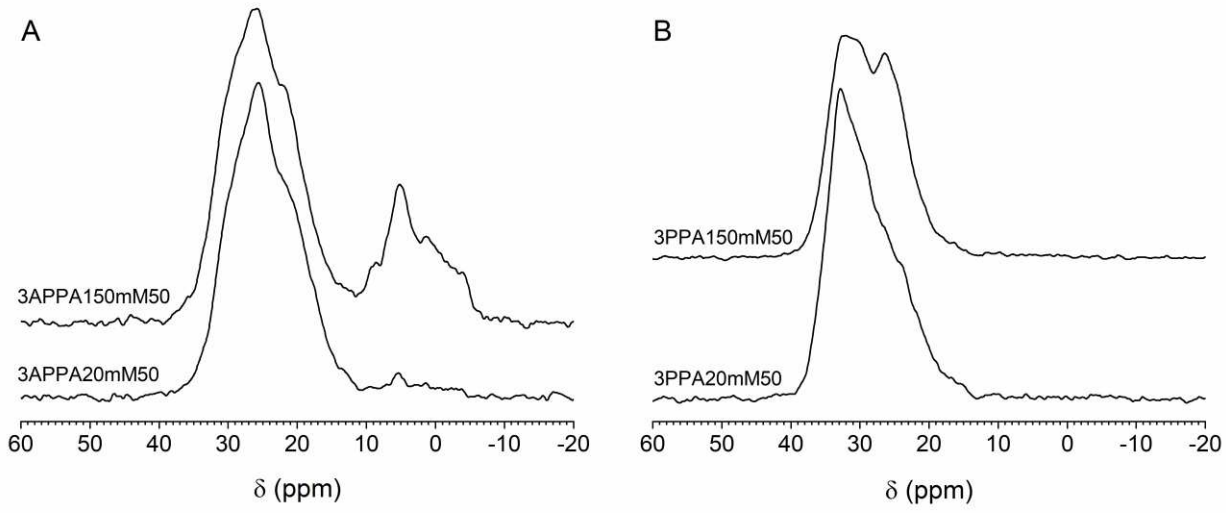

Figure 7: ^{31}P CP-MAS NMR spectra of 3APPA grafted samples (A) and 3PPA grafted samples (B).

In addition, also a broad band of multiple signals/shoulders is observed for sample 3APPA150mM50 in the region between -10 and 10 ppm composed of different contributing resonances, but with a main resonance around 5 ppm. The large upfield shift of these resonance signals indicates the formation of P environments with an increased shielding and can possibly be assigned to the presence of layered (crystalline) titanium aminophosphonate based structures, formed by a dissolution-precipitation reaction at the surface. To the knowledge of the authors, such structures have not yet been described or reported in literature upon surface grafting with 3APPA. For the grafting of alkyl PAs, it is known that titanium phosphonate formation is enhanced under harsh synthesis conditions (combination of high temperature and concentration). The presence of such structures has already been evidenced by TEM and by the presence of a resonance signal between -4 and 8 ppm in ^{31}P NMR depending on the nature of the organic group (i.e. aliphatic vs aromatic).[59,113,114] However, such layered titanium propylphosphonate structures are absent for both 3PPA modifications, as shown in Figure 7B.

4. Conclusions

This study provides in-depth knowledge on the impact of the amine group on the grafting of 3-aminopropylphosphonic acid (3APPA) on Hombikat M311 by comparison with propylphosphonic acid (3PPA) as an amine-free structural analogue, via a combination of experimental- and computational work. Spectroscopic investigations (DRIFT, XPS and ^{31}P CP-MAS NMR) on 3APPA and 3PPA grafted samples combined with DFT calculations on clean- and hydrated surfaces, reveal the peculiar behavior of 3APPA and the complexity and variety of conformational modes of the aminopropyl chain at the TiO_2 surface.

Modification degrees between 0.6 and 1.4 #/nm² and 0.6 and 1.1 #/nm² are obtained for 3PPA and 3APPA, respectively. Increasing the concentration and temperature results in an increased modification degree. At 50 °C, similar modification degrees for 3PPA and 3APPA are obtained for a given concentration, while at 90 °C, lower modification degrees are obtained for 3APPA compared to 3PPA. As the competitive adsorption with water is lower at 90 °C than at 50 °C for both precursors, the lower modification degree of 3APPA already suggests that the amine group induces additional surface interactions that are absent for 3PPA. This is supported by differences in peak position and relative intensities of the broad bands in the P–O region (1300-900 cm^{-1}) in DRIFT.

The different experimental techniques reveal the presence of different chemical states and conformations of the amine functional group. The interference of surface adsorbed water in DRIFT hampers the determination of the relative contributions of the amine speciation, impeding the correlation with the modification conditions. Semi-quantitative information on the amine speciation is obtained from XPS, where contributions of NH_2 and NH_3^+ chemical states were found in the N1s in a constant fraction of 65% and 35%, respectively, irrespective

of the modification conditions. However, these fractions only give averaged information on the chemical states of the amine functionality, since hydrogen bonded amine groups are also present, of which their binding energy strongly depends on the hydrogen bonding strength.

Based on DFT calculations on the predominant anatase crystal facet (101), the presence of a intra – and inter adsorbate and adsorbate-surface interactions have been revealed for 3APPA, with a stabilization of each modelled structure with increasing number of adsorbed water molecules. The corresponding decrease in adsorption energy is independent on the presence of the amine group, given a similar stabilization observed for 3PPA, evidencing that the presence of water on anatase (101) intrinsically results in the stabilization of an organophosphonic acid adsorption complex. On a fully hydrated surface (i.e. reaching monolayer coverage of water), which approximates more closely the hydration state under real experimental conditions, the differences in adsorption energy between the 3APPA modelled structures are too small to make a decisive statement on the presence of preferred conformations. This is in line with the calculated ^{31}P NMR chemical shifts associated with the studied structures, which coincide with the broad band (35-12 ppm) found in the experimental spectra.

The complementary approach of experimental and computational techniques reveals a complex interaction of 3APPA with the titania surface involving multiple adsorption geometries but without the ability to differentiate between structures nor in their order of relative occurrence. The surface modification at a high 3APPA concentration (150mM) results in the presence of a second broad band in the ^{31}P NMR spectra between -10 and 10 ppm. Although this region can only be tentatively ascribed to the presence of layered titanium aminophosphonate-type structures, a different phosphorus environment is clearly present due

to a different nature of interaction between 3APPA and the titania surface in addition to surface grafting.

The coexistence of multiple interaction sites and chemical states of the amine group might have consequences on their behavior in different applications. Moreover, a difference in conformation is to be expected depending on the solvent environment, here represented by the impact of water. As the amine group is (partly) involved in hydrogen bonding or other surface interactions, its accessibility for adsorption of molecules or subsequent conjugation reactions might be hindered or altered. Knowledge on the impact of this competitive interaction is of high interest for further research.

Acknowledgments

This work is supported by the Research Foundation Flanders (FWO) via the Hercules project (AUHL/15/2 - GOH3816N). All calculations were performed using the Hopper HPC infrastructure at the CalcUA core facility of the University of Antwerp, a division of the Flemish Supercomputer Center VSC, funded by the Hercules Foundation, the Flemish Government (department EWI) and the University of Antwerp. Furthermore, the authors would like to acknowledge S. Defossé and K. Leyssens for the N_2 sorption measurements, W. Brusten and K. Duyssens for the ICP measurements, R. Kemps for the SEM measurements and M. Mertens for the XRD measurements.

CRediT authorship contribution statement

Nick Gys: Conceptualization, Methodology, Validation, Investigation, Writing-original draft, Visualization. **Laurens Siemons (calculations)**: Methodology, Validation, Investigation, Writing-review & editing, Visualization. **Bram Pawlak (NMR)**: Methodology, Validation, Investigation, Writing-review & editing. **Kenny Wyns**: Methodology, Validation, Investigation. **Kitty Baert (XPS)**: Methodology, Validation, Investigation, Writing-review &

editing, Visualization. **Tom Hauffman (XPS)**: Methodology, Writing-review & editing, Supervision. **Peter Adriaensens (NMR)**: Methodology, Writing-review & editing, Supervision. **Franck Blockhuys (calculations)**: Methodology, Validation, Investigation, Writing-review & editing, Supervision. **Bart Michielsen**: Conceptualization, Methodology, Writing-review & editing, Supervision. **Steven Mullens**: Conceptualization, Methodology, Writing-review & editing, Supervision. **Vera Meynen**: Conceptualization, Methodology, Writing-review & editing, Supervision

5. References

1. Terra, J. C. S., Moores, A. & Moura, F. C. C. Amine-Functionalized Mesoporous Silica as a Support for on-Demand Release of Copper in the A3-Coupling Reaction: Ultralow Concentration Catalysis and Confinement Effect. *ACS Sustain. Chem. Eng.* **7**, 8696–8705 (2019).
2. Veerakumar, P., Thanasekaran, P., Lu, K. L., Liu, S. Bin & Rajagopal, S. Functionalized Silica Matrices and Palladium: A Versatile Heterogeneous Catalyst for Suzuki, Heck, and Sonogashira Reactions. *ACS Sustainable Chemistry and Engineering* **5**, 6357–6376 (2017).
3. Abney, C. W., Mayes, R. T., Saito, T. & Dai, S. Materials for the Recovery of Uranium from Seawater. *Chem. Rev.* **117**, 13935–14013 (2017).
4. Sharma, S., Krishna Kumar, A. S. & Rajesh, N. A perspective on diverse adsorbent materials to recover precious palladium and the way forward. *RSC Adv.* **7**, 52133–52142 (2017).
5. Florek, J., Giret, S., Juère, E., Larivière, D. & Kleitz, F. Functionalization of mesoporous materials for lanthanide and actinide extraction. *Dalt. Trans.* **45**, 14832–14854 (2016).
6. Mustafa, G., Wyns, K., Vandezande, P., Buekenhoudt, A. & Meynen, V. Novel grafting method efficiently decreases irreversible fouling of ceramic nanofiltration membranes. *J. Memb. Sci.* **470**, 369–377 (2014).
7. Mustafa, G., Wyns, K., Buekenhoudt, A. & Meynen, V. New insights into the fouling mechanism of dissolved organic matter applying nanofiltration membranes with a variety of surface chemistries. *Water Res.* **93**, 195–204 (2016).
8. Croissant, J. G., Fatieiev, Y., Almalik, A. & Khashab, N. M. Mesoporous Silica and Organosilica Nanoparticles: Physical Chemistry, Biosafety, Delivery Strategies, and Biomedical Applications. *Adv. Healthc. Mater.* **7**, 1–75 (2018).
9. Kesse, S. *et al.* Mesoporous silica nanomaterials: Versatile nanocarriers for cancer theranostics and drug and gene delivery. *Pharmaceutics* **11**, 1–26 (2019).
10. Knežević, N., Gadjanski, I. & Durand, J. O. Magnetic nanoarchitectures for cancer sensing, imaging and therapy. *J. Mater. Chem. B* **7**, 9–23 (2019).
11. Ahmadi, E., Dehghannejad, N., Hashemikia, S., Ghasemnejad, M. & Tabebordbar, H. Synthesis and surface modification of mesoporous silica nanoparticles and its application as carriers for sustained drug delivery. *Drug Deliv.* **21**, 164–172 (2014).
12. Vall, M. *et al.* Effects of amine modification of mesoporous magnesium carbonate on controlled drug release. *Int. J. Pharm.* (2017). doi:10.1016/j.ijpharm.2017.03.063
13. Ossipov, D. A. Bisphosphonate-modified biomaterials for drug delivery and bone tissue engineering. *Expert Opin. Drug Deliv.* **12**, 1443–1458 (2015).
14. Hoffmann, F., Cornelius, M., Morell, J. & Fröba, M. Silica-based mesoporous organic-inorganic hybrid materials. *Angew. Chemie - Int. Ed.* **45**, 3216–3251 (2006).
15. Soltani, S., Khanian, N., Rashid, U. & Yaw Choong, T. S. Fundamentals and recent progress relating to the fabrication, functionalization and characterization of mesostructured materials using diverse synthetic methodologies. *RSC Adv.* **10**, 16431–16456 (2020).
16. Gu, D. & Schüth, F. Synthesis of non-siliceous mesoporous oxides. *Chem. Soc. Rev.* **43**, 313–344 (2014).
17. Nawrocki, J. *et al.* Part I. Chromatography using ultra-stable metal oxide-based stationary phases for

HPLC. *J. Chromatogr. A* **1028**, 31–62 (2004).

18. Claessens, H. A. & Van Straten, M. A. Review on the chemical and thermal stability of stationary phases for reversed-phase liquid chromatography. *J. Chromatogr. A* **1060**, 23–41 (2004).
19. Zhang, Y. *et al.* Titanate and titania nanostructured materials for environmental and energy applications: A review. *RSC Adv.* **5**, 79479–79510 (2015).
20. Mahdavi-Shakib, A. *et al.* Titania surface chemistry and its influence on supported metal catalysts. *Polyhedron* **170**, 41–50 (2019).
21. Noman, M. T., Ashraf, M. A. & Ali, A. Synthesis and applications of nano-TiO 2 : a review. *Environ. Sci. Pollut. Res.* **26**, 3262–3291 (2019).
22. Ge, M. *et al.* A review of TiO2 nanostructured catalysts for sustainable H2 generation. *Int. J. Hydrogen Energy* **42**, 8418–8449 (2017).
23. Pujari, S. P., Scheres, L., Marcelis, A. T. M. & Zuilhof, H. Covalent surface modification of oxide surfaces. *Angew. Chemie - Int. Ed.* **53**, 6322–6356 (2014).
24. Meynen, V., Castricum, H. & Buekenhoudt, A. Class II Hybrid Organic-inorganic Membranes Creating New Versatility in Separations. *Curr. Org. Chem.* **18**, 2334–2350 (2014).
25. Van Heetvelde, P. *et al.* A new method to graft titania using Grignard reagents. *Chem. Commun.* **49**, 6998–7000 (2013).
26. Van Dijck, J. G. *et al.* Synthesis – properties correlation and the unexpected role of the titania support on the Grignard surface modification. *Appl. Surf. Sci.* **527**, (2020).
27. Marcinko, S. & Fadeev, A. Y. Hydrolytic stability of organic monolayers supported on TiO2 and ZrO2. *Langmuir* **20**, 2270–2273 (2004).
28. Queffélec, C., Petit, M., Janvier, P., Knight, D. A. & Bujoli, B. Surface Modification Using Phosphonic Acids and Esters. *Chem. Rev.* **112**, 3777–3807 (2012).
29. Guerrero, G., Alauzun, J. G., Granier, M., Laurencin, D. & Mutin, P. H. Phosphonate coupling molecules for the control of surface/interface properties and the synthesis of nanomaterials. *Dalt. Trans.* **42**, 12569–12585 (2013).
30. Boissezon, R., Muller, J., Beaugeard, V., Monge, S. & Robin, J. J. Organophosphonates as anchoring agents onto metal oxide-based materials: Synthesis and applications. *RSC Adv.* **4**, 35690–35707 (2014).
31. Merlet, R. B., Pizzoccaro-Zilamy, M. A., Nijmeijer, A. & Winnubst, L. Hybrid ceramic membranes for organic solvent nanofiltration: State-of-the-art and challenges. *J. Memb. Sci.* **599**, 117839 (2020).
32. Hao, P., Schwartz, D. K. & Medlin, J. W. Phosphonic acid promotion of supported Pd catalysts for low temperature vanillin hydrodeoxygenation in ethanol. *Appl. Catal. A Gen.* **561**, 1–6 (2018).
33. Coan, P. D., Griffin, M. B., Ciesielski, P. N. & Medlin, J. W. Phosphonic acid modifiers for enhancing selective hydrodeoxygenation over Pt catalysts: The role of the catalyst support. *J. Catal.* **372**, 311–320 (2019).
34. Ellis, L. D., Ballesteros-Soberanas, J., Schwartz, D. K. & Medlin, J. W. Effects of metal oxide surface doping with phosphonic acid monolayers on alcohol dehydration activity and selectivity. *Appl. Catal. A Gen.* **571**, 102–106 (2019).
35. Zhang, J., Deo, S., Janik, M. J. & Will Medlin, J. Control of Molecular Bonding Strength on Metal Catalysts with Organic Monolayers for CO2 Reduction. *J. Am. Chem. Soc.* **142**, 5184–5193 (2020).

36. Paniagua, S. A. *et al.* Phosphonic Acids for Interfacial Engineering of Transparent Conductive Oxides. *Chem. Rev.* **116**, 7117–7158 (2016).
37. Randon, J. & Paterson, R. Preliminary studies on the potential for gas separation by mesoporous ceramic oxide membranes surface modified by alkyl phosphonic acids. *J. Memb. Sci.* **134**, 219–223 (1997).
38. He, H. B., Feng, Y. Q., Qu-Li, Da, S. L. & Hu, Z. X. Preparation and evaluation of n-octadecylphosphonic acid-modified magnesia-zirconia stationary phases for reversed-phase liquid chromatography. *Anal. Chim. Acta* **542**, 268–279 (2005).
39. He, H. B., Feng, Y. Q., Da, S. L., Hu, Z. X. & Qu, L. High-performance liquid chromatography of some basic drugs on a n-octadecylphosphonic acid modified magnesia-zirconia stationary phase. *J. Sep. Sci.* **28**, 1577–1586 (2005).
40. Ding, J., Gao, Q., Luo, D., Shi, Z. G. & Feng, Y. Q. n-Octadecylphosphonic acid grafted mesoporous magnetic nanoparticle: Preparation, characterization, and application in magnetic solid-phase extraction. *J. Chromatogr. A* **1217**, 7351–7358 (2010).
41. Mutin, P. H. & Guerrero, G. Hybrid materials from organophosphorus coupling molecules. *J. Mater. Chem.* **15**, 3761–3768 (2005).
42. Mutin, P. H., Guerrero, G. & Vioux, A. Organic-inorganic hybrid materials based on organophosphorus coupling molecules: From metal phosphonates to surface modification of oxides. *Comptes Rendus Chimie* **6**, 1153–1164 (2003).
43. Brodard-severac, F. *et al.* High-Field O MAS NMR Investigation of Phosphonic Acid Monolayers on Titania. *Chem. Mater.* 5191–5196 (2008).
44. Geldof, D. *et al.* Binding modes of phosphonic acid derivatives adsorbed on TiO2surfaces: Assignments of experimental IR and NMR spectra based on DFT/PBC calculations. *Surf. Sci.* **655**, 31–38 (2017).
45. Tielens, F. *et al.* Characterization of Phosphate Species on Hydrated Anatase TiO2 Surfaces. *Langmuir* **32**, 997–1008 (2016).
46. Ferreira, J. M., Marcinko, S., Sheardy, R. & Fadeev, A. Y. Calorimetric study of the reactions of n-alkylphosphonic acids with metal oxide surfaces. *J. Colloid Interface Sci.* **286**, 258–262 (2005).
47. Spori, D. M. *et al.* Influence of alkyl chain length on phosphate self-assembled monolayers. *Langmuir* **23**, 8053–8060 (2007).
48. Quiñones, R., Raman, A. & Gawalt, E. S. Functionalization of nickel oxide using alkylphosphonic acid self-assembled monolayers. *Thin Solid Films* **516**, 8774–8781 (2008).
49. Lassiaz, S. *et al.* Organo-lined alumina surface from covalent attachment of alkylphosphonate chains in aqueous solution. *New J. Chem.* **34**, 1424–1435 (2010).
50. Fonder, G. *et al.* Anchoring of alkylphosphonic derivatives molecules on copper oxide surfaces. *Appl. Surf. Sci.* **257**, 6300–6307 (2011).
51. De Pauli, M. *et al.* Thermal stability and ordering study of long- and short-alkyl chain phosphonic acid multilayers. *Langmuir* **28**, 15124–15133 (2012).
52. Sang, L. *et al.* Effect of time and deposition method on quality of phosphonic acid modifier self-assembled monolayers on indium zinc oxide. *Appl. Surf. Sci.* **389**, 190–198 (2016).
53. Skibinski, E. S., Debenedetti, W. J. I. & Hines, M. A. Solution Deposition of Phenylphosphinic Acid Leads to Highly Ordered, Covalently Bound Monolayers on TiO2(110) Without Annealing. *J. Phys.*

Chem. C **121**, 14213–14221 (2017).

54. Wagstaffe, M. *et al.* An Experimental Investigation of the Adsorption of a Phosphonic Acid on the Anatase TiO $_2$ (101) Surface. *J. Phys. Chem. C* **120**, 1693–1700 (2016).
55. Di Valentin, C. & Costa, D. Anatase TiO 2 surface functionalization by alkylphosphonic acid: A DFT+D study. *J. Phys. Chem. C* **116**, 2819–2828 (2012).
56. Luschtinetz, R., Frenzel, J., Milek, T. & Seifert, G. Adsorption of phosphonic acid at the tio2 anatase (101) and rutile (110) surfaces. *J. Phys. Chem. C* **113**, 5730–5740 (2009).
57. Nilsing, M., Lunell, S., Persson, P. & Ojamäe, L. Phosphonic acid adsorption at the TiO2 anatase (1 0 1) surface investigated by periodic hybrid HF-DFT computations. *Surf. Sci.* **582**, 49–60 (2005).
58. O'Rourke, C. & Bowler, D. R. DSSC anchoring groups: A surface dependent decision. *J. Phys. Condens. Matter* **26**, (2014).
59. Roevens, A. *et al.* Revealing the influence of the solvent in combination with temperature, concentration and pH on the modification of TiO2 with 3PA. *Mater. Chem. Phys.* **184**, 324–334 (2016).
60. Roevens, A. *et al.* Aqueous or solvent based surface modification: The influence of the combination solvent – organic functional group on the surface characteristics of titanium dioxide grafted with organophosphonic acids. *Appl. Surf. Sci.* **416**, 716–724 (2017).
61. Guerrero, G., Mutin, P. H. & Vioux, A. Anchoring of phosphonate and phosphinate coupling molecules on titania particles. *Chem. Mater.* **13**, 4367–4373 (2001).
62. Feichtenschlager, B., Lomoschitz, C. J. & Kickelbick, G. Tuning the self-assembled monolayer formation on nanoparticle surfaces with different curvatures: Investigations on spherical silica particles and plane-crystal-shaped zirconia particles. *J. Colloid Interface Sci.* **360**, 15–25 (2011).
63. Gharbi, K. *et al.* Alkyl phosphonic acid-based ligands as tools for converting hydrophobic iron nanoparticles into water soluble iron-iron oxide core-shell nanoparticles. *New J. Chem.* **41**, 11898–11905 (2017).
64. Tudisco, C. *et al.* Multifunctional magnetic nanoparticles for enhanced intracellular drug transport. *J. Mater. Chem. B* **3**, 4134–4145 (2015).
65. Tudisco, C., Oliveri, V., Cantarella, M., Vecchio, G. & Condorelli, G. G. Cyclodextrin anchoring on magnetic Fe 3O 4 nanoparticles modified with phosphonic linkers. *Eur. J. Inorg. Chem.* 5323–5331 (2012). doi:10.1002/ejic.201200510
66. Aquino, C. C. *et al.* Amine-functionalized titania-based porous structures for carbon dioxide postcombustion capture. *J. Phys. Chem. C* **117**, 9747–9757 (2013).
67. Seisenbaeva, G. A. *et al.* Molecular insight into the mode-of-action of phosphonate monolayers as active functions of hybrid metal oxide adsorbents. Case study in sequestration of rare earth elements. *RSC Adv.* **5**, 24575–24585 (2015).
68. Li, P. *et al.* In-situ preparation of amino-terminated dendrimers on TiO 2 films by generational growth for potential and efficient surface functionalization. *Appl. Surf. Sci.* **459**, 438–445 (2018).
69. Canepa, P. *et al.* Anchoring of Aminophosphonates on Titanium Oxide for Biomolecular Coupling. *J. Phys. Chem. C* **123**, 16843–16850 (2019).
70. Ramsier, R. D., Henriksen, P. N. & Gent, A. N. Adsorption of phosphorus acids on alumina. *Surf. Sci.* **203**, 72–88 (1988).

71. Wapner, K., Stratmann, M. & Grundmeier, G. Structure and stability of adhesion promoting aminopropyl phosphonate layers at polymer/aluminium oxide interfaces. *Int. J. Adhes. Adhes.* **28**, 59–70 (2008).
72. Pa-Zik, R. *et al.* Surface functionalization of the metal oxide nanoparticles with biologically active molecules containing phosphonate moieties. Case study of BaTiO3. *J. Phys. Chem. C* **115**, 9850–9860 (2011).
73. Shanmugam, N. R., Muthukumar, S. & Prasad, S. Surface modification of ZnO nanostructured electrodes with thiol and phosphonic acid moieties for biosensing applications. *Anal. Methods* **9**, 5525–5533 (2017).
74. Giannozzi, P. *et al.* QUANTUM ESPRESSO: A modular and open-source software project for quantum simulations of materials. *J. Phys. Condens. Matter* **21**, (2009).
75. Wu, Z. & Cohen, R. E. More accurate generalized gradient approximation for solids. *Phys. Rev. B - Condens. Matter Mater. Phys.* **73**, 2–7 (2006).
76. Tran, F., Laskowski, R., Blaha, P. & Schwarz, K. Performance on molecules, surfaces, and solids of the Wu-Cohen GGA exchange-correlation energy functional. *Phys. Rev. B - Condens. Matter Mater. Phys.* **75**, 1–14 (2007).
77. Blöchl, P. E. Projector augmented-wave method. *Phys. Rev. B* **50**, 17953–17979 (1994).
78. Grimme, S. Semiempirical GGA-Type Density Functional Constructed with a Long-Range Dispersion Correction. *J. Comput. Chem.* **32**, 174–182 (2006).
79. Barone, V. Role and Effective Treatment of Dispersive Forces in Materials: Polyethylene and Graphite Crystals as Test Cases. *J. Comput. Chem.* **32**, 174–182 (2009).
80. Björkman, T. CIF2Cell: Generating geometries for electronic structure programs. *Comput. Phys. Commun.* **182**, 1183–1186 (2011).
81. Pickard, C. J. & Mauri, F. All-electron magnetic response with pseudopotentials: NMR chemical shifts. *Phys. Rev. B - Condens. Matter Mater. Phys.* **63**, 2451011–2451013 (2001).
82. Müller, D., Jahn, E., Ladwig, G. & Haubenreisser, U. High-resolution solid-state 27Al and 31P NMR: correlation between chemical shift and mean Al-O-P angle in AlPO4 polymorphs. *Chem. Phys. Lett.* **109**, 332–336 (1984).
83. Gao, W., Dickinson, L., Grozinger, C., Morin, F. G. & Reven, L. Self-Assembled Monolayers of Alkylphosphonic Acids on Metal Oxides. *Langmuir* **12**, 6429–6435 (1996).
84. Guerrero, G., Mutin, P. H. & Vioux, A. Organically modified aluminas by grafting and sol-gel processes involving phosphonate derivatives. *J. Mater. Chem.* **11**, 3161–3165 (2001).
85. Hotchkiss, P. J., Malicki, M., Giordano, A. J., Armstrong, N. R. & Marder, S. R. Characterization of phosphonic acid binding to zinc oxide. *J. Mater. Chem.* **21**, 3107 (2011).
86. Yah, W. O., Takahara, A. & Lvov, Y. M. Selective Modification of Halloysite Lumen with Octadecyl Phosphonic Acid : New Inorganic Tubular Micelle Selective. *J. Am. Chem. Soc.* **134**, 1853–1859 (2012).
87. Shimizu, I. *et al.* Raman scattering study of the interaction of 3-aminopropyltriethoxy silane on silica gel. Time-dependent conformational change of aminopropylsilyl segments. *Vib. Spectrosc.* **14**, 125–132 (1997).
88. Socrates, G. *Infrared and Raman characteristic group frequencies*. *Infrared and Raman characteristic group frequencies* (2004). doi:10.1002/jrs.1238
89. Takeuchi, M., Martra, G., Coluccia, S. & Anpo, M. Investigations of the structure of H2O clusters

adsorbed on TiO2 surfaces by near-infrared absorption spectroscopy. *J. Phys. Chem. B* **109**, 7387–7391 (2005).

90. Morterra, C. An infrared study of anatase properties. *J. Chem. Soc. Faraday Transit. 1* **84**, 1617–1637 (1988).
91. Paul, G. *et al.* Investigating the Interaction of Water Vapour with Aminopropyl Groups on the Surface of Mesoporous Silica Nanoparticles. *ChemPhysChem* **18**, 839–849 (2017).
92. Iliade, P., Miletto, I., Coluccia, S. & Berlier, G. Functionalization of mesoporous MCM-41 with aminopropyl groups by co-condensation and grafting: A physico-chemical characterization. *Res. Chem. Intermed.* **38**, 785–794 (2012).
93. Zhang, L., Liu, J., Yang, J., Yang, Q. & Li, C. Direct synthesis of highly ordered amine-functionalized mesoporous ethane-silicas. *Microporous Mesoporous Mater.* **109**, 172–183 (2008).
94. Calvo, A. *et al.* Mesoporous aminopropyl-functionalized hybrid thin films with modulable surface and environment-responsive behavior. *Chem. Mater.* **20**, 4661–4668 (2008).
95. Chiang, C. H. W. A. N. H. W. A., Ishida, H. & Koenig, J. L. The Structure of y-Aminopropyltriethoxysilane on Glass Surfaces. *J. Colloid Interface Sci.* **74**, 396–404 (1980).
96. Chiang, C. & Koenig, J. L. Fourier transform infrared spectroscopic study of the adsorption of multiple amino silane coupling agents on glass surfaces. *J. Colloid Interface Sci.* **83**, 361–370 (1981).
97. Shimizu, I., Okabayashi, H., Taga, K., Nishio, E. & O'Connor, C. J. Diffuse reflectance infrared Fourier transform spectral study of the thermal and adsorbed-water effects of a 3-aminopropyltriethoxysilane layer modified onto the surface of silica gel. *Vib. Spectrosc.* **14**, 113–123 (1997).
98. Pasternack, R. M., Amy, S. R. & Chabal, Y. J. Attachment of 3-(aminopropyl)triethoxysilane on silicon oxide surfaces: Dependence on solution temperature. *Langmuir* **24**, 12963–12971 (2008).
99. Asahi, R., Morikawa, T., Ohwaki, T., Aoki, K. & Taga, Y. Visible-light photocatalysis in nitrogen-doped titanium oxides. *Science (80-.).* **293**, 269–271 (2001).
100. Ma, T., Akiyama, M., Abe, E. & Imai, I. High-efficiency dye-sensitized solar cell based on a nitrogen-doped nanostructured titania electrode. *Nano Lett.* **5**, 2543–2547 (2005).
101. Spadavecchia, F. *et al.* Second generation nitrogen doped titania nanoparticles: A comprehensive electronic and microstructural picture. *Chinese J. Chem.* **32**, 1195–1213 (2014).
102. Wielant, J., Hauffman, T., Blajiev, O., Hausbrand, R. & Terryn, H. Influence of the iron oxide acid-base properties on the chemisorption of model epoxy compounds studied by XPS. *J. Phys. Chem. C* **111**, 13177–13184 (2007).
103. Gadois, C., Światowska, J., Zanna, S. & Marcus, P. Influence of titanium surface treatment on adsorption of primary amines. *J. Phys. Chem. C* **117**, 1297–1307 (2013).
104. Abrahami, S. T., Hauffman, T., De Kok, J. M. M., Mol, J. M. C. & Terryn, H. XPS Analysis of the Surface Chemistry and Interfacial Bonding of Barrier-Type Cr(VI)-Free Anodic Oxides. *J. Phys. Chem. C* **119**, 19967–19975 (2015).
105. Hemeryck, A., Motta, A., Lacaze-Dufaure, C., Costa, D. & Marcus, P. DFT-D study of adsorption of diaminoethane and propylamine molecules on anatase (101) TiO 2 surface. *Appl. Surf. Sci.* **426**, 107–115 (2017).
106. Sun, C., Liu, L. M., Selloni, A., Lu, G. Q. & Smith, S. C. Titania-water interactions: A review of

theoretical studies. *J. Mater. Chem.* **20**, 10319–10334 (2010).

107. Martinez-Casado, R., Mallia, G., Harrison, N. M. & Pérez, R. First-Principles Study of the Water Adsorption on Anatase(101) as a Function of the Coverage. *J. Phys. Chem. C* **122**, 20736–20744 (2018).
108. Mino, L., Cesano, F., Scarano, D., Spoto, G. & Martra, G. Molecules and heterostructures at TiO2 surface: the cases of H2O, CO2, and organic and inorganic sensitizers. *Res. Chem. Intermed.* **45**, 5801–5829 (2019).
109. Petersen, T. & Klüner, T. Water Adsorption on Ideal Anatase-TiO2(101) - An Embedded Cluster Model for Accurate Adsorption Energetics and Excited State Properties. *Zeitschrift fur Phys. Chemie* **234**, 813–834 (2020).
110. Harris, R. K., Merwin, L. H. & Hägele, G. Solid-state NMR study of a series of aminophosphonic acids. *Magn. Reson. Chem.* **27**, 470–475 (1989).
111. Glowacki, Z., Hoffmann, M., Topolski, M. & Rachon, J. Substituent effects on the 31P NMR chemical shifts of 1-amino-and 1-hydroxy-alkylphosphonic acids. *Phosphorus. Sulfur. Silicon Relat. Elem.* **51**, 227 (1990).
112. Tassi, M. *et al.* A detailed investigation of the microwave assisted phenylphosphonic acid modification of P25 TiO2. *Adv. Powder Technol.* **28**, 236–243 (2017).
113. Roevens, A. In-depth study of organophosphonic acid modification on titania. (2017).
114. Tassi, M., Reekmans, G., Carleer, R. & Adriaensens, P. Fully quantitative description of hybrid TiO2 nanoparticles by means of solid state 31P NMR. *Solid State Nucl. Magn. Reson.* **78**, 50–55 (2016).

Table of contents/Abstract Graphic